Slice Acceleration in the 3 Tesla Component of the Human Connectome Project

Kâmil Uğurbil[1]; Edward J. Auerbach[1]; Steen Moeller[1]; Junqian Xu[4]; An Vu[1]; Matthew F. Glasser[3]; Christophe Lenglet[1]; Stamatios N. Sotiropoulos[2]; Stephen M. Smith[2]; Timothy EJ Behrens[2]; David Van Essen[3]; Essa Yacoub[1]

[1] Center for Magnetic Resonance Research (CMRR), University of Minnesota, Minneapolis, MN, USA
[2] Oxford Centre for Functional MRI of the Brain (FMRIB), University of Oxford, UK
[3] Department of Anatomy & Neurobiology, Washington University School of Medicine, St. Louis, MO, USA
[4] Translational and Molecular Imaging Institute, Icahn School of Medicine at Mount Sinai, New York, NY, USA

Introduction

The Human Connectome Project (HCP) was launched on the principle of undertaking significant new advances in magnetic resonance (MR) based imaging of the human brain and using these advanced technologies to generate to-date the most complete and accurate description of the connections among gray matter locations in the human brain at the millimeter scale.

At the time HCP was initiated, a growing number of studies had revealed important insights through systematic studies of whole-brain connectivity (e.g. [1-6]) using resting-state functional magnetic resonance imaging (rfMRI) and diffusion imaging (dMRI). rfMRI uses correlations in the spontaneous temporal fluctuations in an fMRI time series to deduce '*functional connectivity*' (e.g. [7-11]) and, dMRI provides the input for tractography algorithms used for the reconstruction of the complex axonal fiber architecture so as to infer '*structural connectivity*' (e.g. reviews [12, 13]). Despite their promise, however, each of these MR methods faces serious technical *limitations*. These include a high incidence of false positives and false negatives [13, 14] that arise from the indirect nature of functional imaging signals [15], dependence on neurovascular coupling [16], the presence of confounding long-range correlations of vascular origin [17], and the complexity of water diffusion in the microenvironment of the brain (e.g. [18, 19]). Given these neurobiological and neurophysiological challenges, undertaking significant new methodological developments to overcome or ameliorate these limitations was considered imperative for the success of the HCP.

A primary challenge in the fMRI component of the HCP is the ability

1

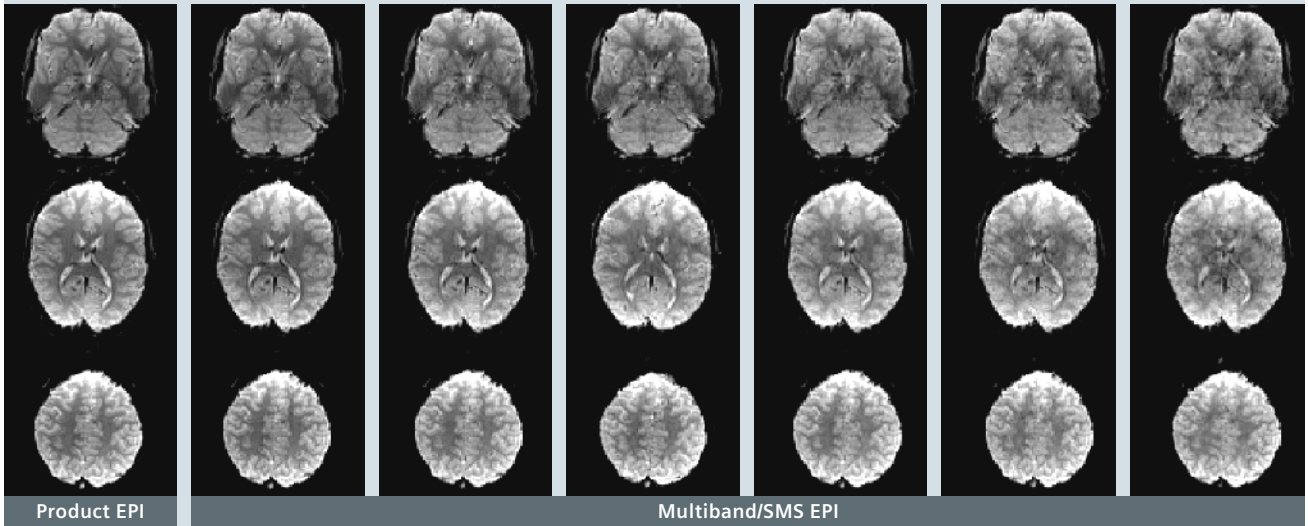

1 Slice accelerated Multiband/SMS images from the HCP obtained at 3T at different acceleration factors. Three slices from a 2 mm isotropic resolution, 64 slice whole brain data set obtained with slice acceleration up to MB factor of 12. For comparison, images were acquired with the same TR (4.8 s) based on the minimum TR attainable with standard EPI (i.e. MB = 1). The example axial slices shown were not from the same MB slice group. Achievable TR at a given MB factor is listed below the MB factors given to show the acceleration potential. *Adapted from Uğurbil et al. 2013 [24], and Xu et al., 2013 [36].*

to capture functional mapping signals with the highest possible fidelity to the underlying gray/white matter neuronal architecture. Therefore, improving spatial resolution for the HCP data was one of the targets set out by the HCP investigators from the inception of the project. However, there is always a compromise between spatial resolution and the total volume acquisition time. Higher spatial resolution requires larger number of slices to cover the volume-of-interest (in the HCP, the whole human brain) and hence leads to a longer TR. Longer TRs are not desirable in fMRI; if they become significantly longer than the T1, image signal-to-noise ratio (SNR) per unit time suffers. In addition, slower acquisitions undermine the accurate sampling of the basal fluctuations in an fMRI time series, potentially degrading efforts to clean up the time series of undesirable sources of fluctuations (such as those induced by respiration and cardiac pulsation), and lead to fewer samples within a given total acquisition time, reducing the statistical power in the analysis of the time series. Thus, it was critical to accelerate the data acquisition rate without significantly impacting image SNR.

Accelerating image acquisition is also critical for dMRI. Improvements in SNR per unit time enable higher spatial resolution without commensurately longer data acquisition times, and/or allow for more extensive sampling of the diffusion encoding space (i.e. q-space, defined by the magnitude and orientations of the diffusion-weighting gradients) so as to more accurately estimate the orientation of white matter fiber bundles, especially in regions where multiple fiber bundles intersect one another at various angles or where fiber bundles bend or fan out and split into multiple trajectories.

In this article, we briefly review the technical developments undertaken for data acquisition at 3 Tesla within the Washington University-University of Minnesota (WU-Minn) Consortium of the HCP (http://humanconnectome.org), composed primarily of three institutions, Washington University, University of Minnesota, Center for Magnetic Resonance Research (CMRR), and Oxford University. An accompanying article by Yacoub et al. in this issue of MAGNETOM Flash describes a parallel effort at 7 Tesla within this consortium. An overview of the overall HCP project is discussed in [20] and more comprehensive and detailed accounts of improvements and optimizations are given in references [21-25].

Pushing image acquisition speed

Improving fMRI data acquisition speed, while critical for the HCP, is relevant to human neuroimaging in general and was already recognized in work prior to the HCP for very high-resolution fMRI applications at ultrahigh magnetic fields [26, 27]. Motivated by the prospect of whole-brain, very high resolution functional mapping at 7T, Moeller et al. [26, 27] used multi-slice GRE EPI[1] at 7T with concurrent accelerations along both the slice and in-plane phase-encode directions, achieving 16-fold two-dimensional acceleration. Multiple slices were simultaneously excited using multiband RF pulses; the signals generated by these multiple slices were acquired simultaneously in a single EPI echo train, with *k*-space undersampling in the phase-encode direction. These simultaneously acquired slices were unaliased using parallel imaging principles and the coil sensitivity profiles of the multichannel receive array employed for data collection. Excellent functional maps at 7T with 1.5 mm isotropic resolution and 88 slices in 1.25 s, or 1 x 1 x 2 mm^3 resolution with 90 slices in 1.5 s were achieved [26, 27].

The use of multiband excitation pulses to simultaneously excite and collect multiple slices (referred to as Multiband (MB) or Simultaneous Multi-Slice (SMS) technique interchangeably) dates back to 2001, when it was demonstrated using gradient recalled echoes, collecting a single *k*-space line at a time (i.e. FLASH), imaging a leg with a spine coil [28]. This approach was further advanced with the introduction of the CAIPIRINHA (Controlled Aliasing In Parallel Imaging Results IN Higher Acceleration) [29, 30] concept where unaliasing of slices was improved significantly by manipulating the phase of the RF excitation pulses progressively for each *k*-space line, so as to effectively shift the simultaneously acquired slices relative to each other in the phase-encoding direction. These earlier initiatives did not catch the attention of the neuroimaging community. However, Moeller at al. [26, 27] demonstrated an application where such rapid volume coverage using Multiband/SMS EPI is critical, thus catalyzing a major interest in this approach. Subsequently, a modified 'blip' strategy in Multiband/SMS EPI, termed 'blipped-CAIPIRINHA', that balances the blips so as to minimize the voxel tilting of the earlier blipping implementation [31] was introduced [32, 33], providing major improvements in *g*-factor noise and achievable slice accelerations, adding to the attractiveness of the approach in EPI based techniques such as fMRI and dMRI.

Initial efforts in the WU-Minn consortium also tried to accelerate beyond what was feasible with Multiband/SMS EPI by combining it with the SIR approach [34], a technique we referred to as Multiplexed-EPI (M-EPI) [35]. A similar combination was also described in an abstract the same year [32]. Multiplexed EPI essentially takes the SIR sequence, where ***s*** RF pulses are applied sequentially in time leading to temporally resolved echoes from the ***s*** different slices, and makes each RF pulse a multiband pulse with ***m*** bands (where ***m*** and ***s*** are positive integers); the result is simultaneous acquisition of ***m*** times ***s*** (i.e. ***m*** x ***s***) slices in a single echo train that contains both simultaneously acquired as well as temporally shifted echoes. Using this method to accelerate whole-brain coverage, the WU-Minn HCP consortium demonstrated [35] that the statistical significance of the Resting-State Networks (RSNs) detected by high dimensional ICA analysis from rfMRI time series significantly improved, and the normally long acquisition time of dMRI was reduced

[1] The product is still under development and not commercially available yet. Its future availability cannot be ensured.

2-4 fold. However, because of the longer echo trains inherent in SIR, the combined technique is not universally advantageous, and the realizable gains depend on several factors, including spatial resolution, MB acceleration capabilities, desired temporal resolution, and the need for in-plane accelerations. As such, in the HCP, Multiplexed EPI was not employed; rather Multiband/SMS EPI with control aliasing ('blipped-CAIPIRINHA') and *without* the use of in-plane phase-encode acceleration was adapted in the WU-Minn consortium as the sequence for the 3T HCP data acquisition.

An example of the type of Multiband/SMS images with 2 mm isotropic nominal resolution obtained in the initial evaluation phase on the WU-Minn 3T HCP scanner (Connectom-Skyra[2], Siemens Healthcare, Erlangen, Germany) is illustrated in Figure 1 for different MB factors (i.e. the number of simultaneously excited slices, or the slice acceleration factor). For comparison, images from the standard EPI sequence (corresponding to MB = 1) available on the scanner are also provided. Although the TR was kept constant at the value attainable for the MB1 so as to maintain identical contrast in these images, the minimum achievable volume TR to cover the whole brain is also indicated for each MB factor. The data were acquired using a 32-channel standard Siemens head coil. Careful scrutiny of the images indicates that MB = 12 data still show much detailed structure although they clearly display greater artifact level. Figure 2 illustrates 18 slices from a whole-head acquisition comparing standard EPI (MB1) images and MB6 Multiband acquisition at 3T at the same TR; excellent EPI image quality is evident in MB = 6 as well as the standard MB = 1 case.

A quantitative analysis of these data is possible using *g*-factors [36] that reflect noise amplification due to the use of parallel imaging using the formulation developed for in-plane parallel imaging along the phase-encode dimension [37]. However, *g*-factors themselves do not inform about residual aliasing among the simultaneously acquired slices. To address this, we introduced a metric named the *L*-factor (leakage factor) [36, 38] that quantifies residual aliasing.

L-factor maps of residual aliasing are illustrated in Figure 3 for Multiband/SMS EPI imaging with MB = 3, 4, 8 and 12 from data acquisition sequences employed for the HCP. Such maps illustrated that there is no perceptible 'leakage' from the center slice to the two adjacent slices for MB = 3 or 4 and the calculated *L*-factor was 0.03 with or without PE_{SHIFT}. With MB = 8 and 12, there is small leakage (Fig. 3), but not sufficient to impact fMRI data.

The objectives of the WU-Minn HCP consortium entailed not only improved pulse sequences but also implementation on the HCP scanners for efficient, stable and robust performance. Therefore, significant efforts were invested in evaluating the performance of the sequences and the associated image reconstruc-

2

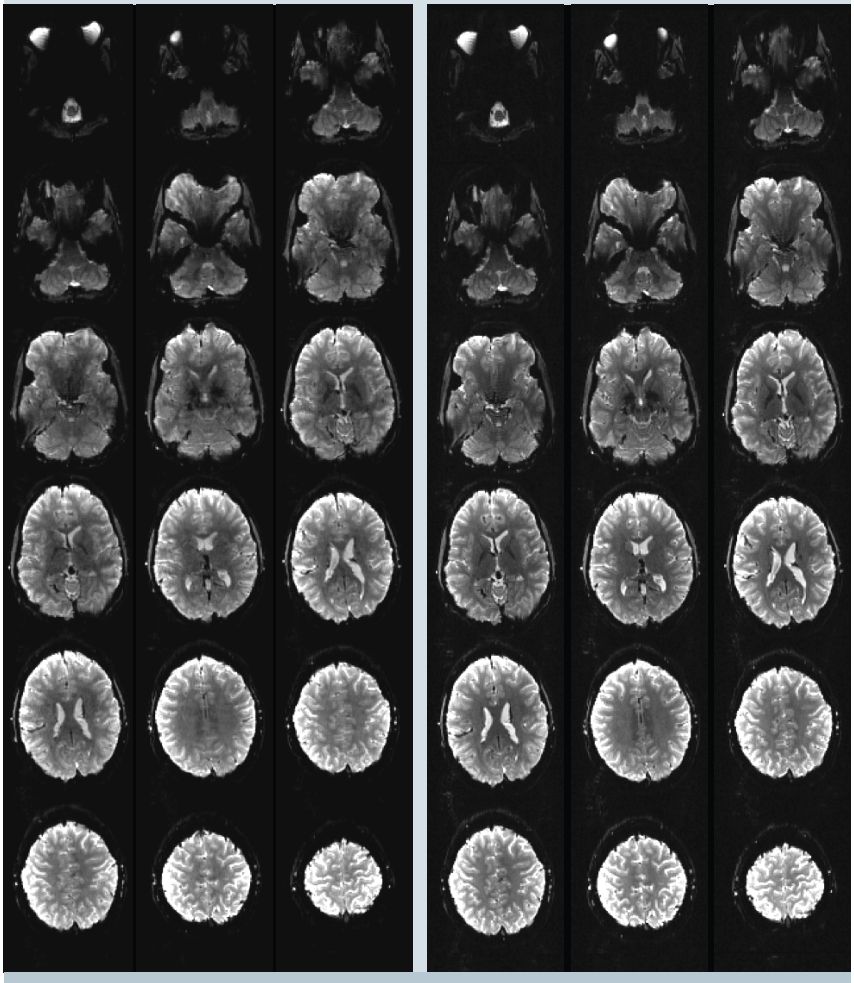

2 Comparing 6-fold slice accelerated Multiband/SMS images at 3T with unaccelerated standard acquisition. Selected slices from a 1.6 mm isotropic, 80 slice whole-brain data set obtained with PE_{SHIFT} = FOV/3, MB factor 6 and standard EPI (MB = 1). TE = 30 ms; 6/8 Partial Fourier along phase-encode direction. TR = 6.7 s for both, set by the minimum TR attainable with MB = 1. Minimum TR that would be possible with MB = 6 acquisition with these parameters would be 1.1 s. Data was obtained with a 32-channel coil on the 3T WU-Minn HCP scanner. *Adapted from Uğurbil et al., 2013 [24] and Xu et al., 2013 [36].*

[2] Product is ongoing research. All data shown are acquired using a non-commercial system under institutional review board permission.

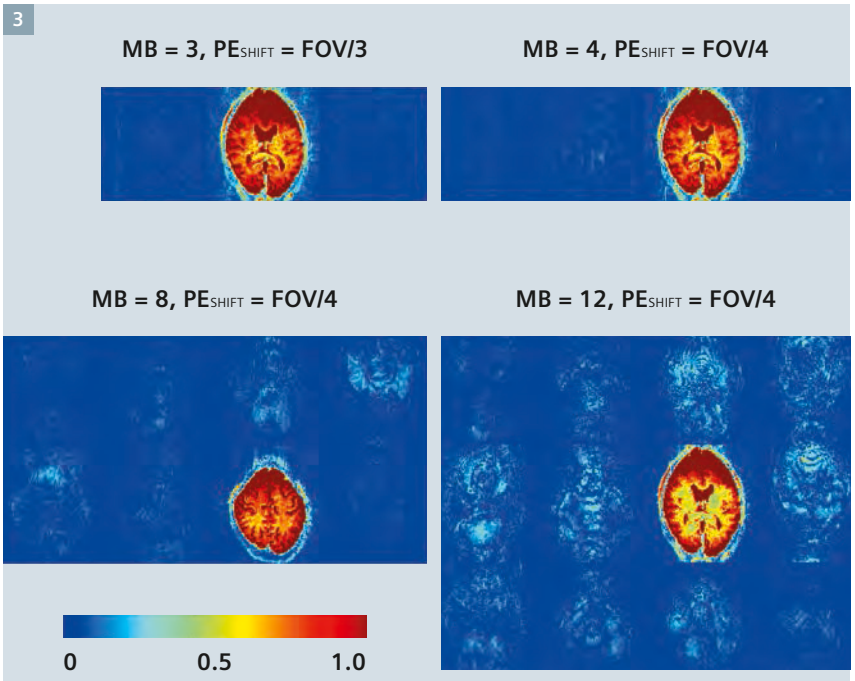

3 Quantifying residual aliasing among simultaneously acquired slices. Signal leakage (*L*-factor) maps showing residual aliasing among simultaneously acquired slices at 3T for MB3, MB4, MB8 and MB12 with PE$_{SHIFT}$. The oscillation imposed on slice (appears in red/yellow color) 'leaks' into other simultaneously acquired slices due to resdiual aliasing. *Adapted from Xu et al. 2013*. We describe the shift induced in the phase-encode direction by controlled aliasing as a fraction of the field-of-view (FOV) and refer to it using the label PE$_{SHIFT}$; thus a PE$_{SHIFT}$ of FOV/4 has a maximal shift of ¼ of the FOV in the phase-encode direction between the simultaneously excited slices. *Adapted from Xu et al. 2013 [36], Moeller et al. 2012 [38].*

Table 1

	rfMRI and tfMRI	dMRI
Multiband Factor (i.e. slice acceleration factor)	8	3
In-plane phase-encode acceleration	None	None
Spatial resolution	2 mm isotropic	1.25 mm isotropic
TE	33 ms	89 ms
TR (whole volume)	0.72 s	5.5 s
Δ	Not applicable	43.1 ms
δ	Not applicable	10.6 ms
q-space sampling	Not applicable	3 shell HARDI b = 1000, 2000, 3000 s/mm^2 270 non-collinear directions

HCP acquisition parameters employed at 3T for fMRI and dMRI.

tion algorithms. The evaluation took place in two stages. The first stage involved evaluation of image quality, temporal stability, noise increase due to parallel imaging, and residual aliasing among the simultaneously excited slices [24]. The second stage examined the performance of the sequences, and the different acquisition parameters for detection of resting-state networks and task activation for fMRI, robustness to subject motion (described in greater detail in [22]), and various metrics for diffusion imaging (also described in greater detail in [21]). Both stages were critical and ultimately led to the final protocol selection [24]. The parameters decided upon for the 3T protocol in the HCP are summarized in Table 1.

The fMRI (both resting-state and task) were run with MB factor of 8 (i.e. 8 fold slice acceleration) at 3T using the 32-channel coil from Siemens Healthcare. Such high slice accelerations are not feasible in dMRI because of peak power limitations and ultimately power deposition (SAR) since dMRI uses spin-echo sequences with nominally 90° and 180° excitation and refocusing pulses, respectively. We qualify the flip angles as 'nominal' because even at 3T and even with a body coil transmission, the flip angle is not uniform in the human head [24]. In fMRI, only an excitation pulse is employed and this pulse is adjusted to lower flip angles (i.e. the Ernst angle) to optimize SNR for the reduced TR made possible with slice acceleration, hence lowering power deposition per pulse. Although methods were developed in the WU-Minn HCP consortium to alleviate the peak power [39] and SAR limitations [40, 41] for Multiband/SMS imaging within the HCP, they were not ready in time to be exhaustively tested for the 3T data collection phase of the WU-Minn HCP. Some of these techniques were, however, adopted in the 7T phase of the project [42].

The HCP 3T protocol does not use in-plane phase encoding acceleration; if possible, we decided to avoid this in order to maximally accelerate the fMRI time series along the slice direction and to avoid the SNR penalty that comes with reduced *k*-space coverage when accelerating along the phase

encode direction. EPI image quality (with the distortion corrections realized by obtaining images with phase-encode running in opposite directions, and also corrected for eddy current effects for dMRI [43, 44]) were considered excellent both for fMRI and dMRI acquisitions [21, 22]. Furthermore, when the performance of 3T dMRI acquisitions with in-plane acceleration was evaluated in terms of fibre crossing sensitivity and uncertainty, they did not perform as well as just using slice acceleration alone. This was likely because of the SNR loss that comes with in-plane phase-encode acceleration.

Rigid body motion of the subject's head is a major problem in the analysis of data from an fMRI time series. As a result, methods for correcting rigid body motion in an fMRI time series by 'realigning' volumetric data is routinely performed in fMRI data analysis. When parallel imaging is employed, the problem of motion becomes more complex because 'reference' or 'calibration' scans that are obtained typically at the beginning of the data collection period and the subsequently acquired accelerated data in the fMRI time series are no longer fully consistent. This problem was evaluated in the HCP fMRI data. The 'conventional' volumetric realignment, which ignores the potential additional problem of a mismatch between the calibration scan and the subsequent images, was found to be surprisingly successful with the Multiband/SMS EPI fMRI data (MB = 8) when motion occurred during the acquisition of the fMRI time series [22]. This likely reflects the fact that coil sensitivity profiles are spatially slowly varying functions. However, motion during the acquisition of the calibration scan when parallel imaging along the phase encoding was employed was a major problem. This confound was not present in the 3T HCP data because phase-encode parallel imaging was not employed; but it was an issue for the 7T HCP data.

Since the 3T component of HCP *does not* use phase encoding acceleration, the calibrations scans are based on single slice versions of the *single-shot* slice selective EPI employed subsequently in the Multiband/SMS acquisition. However, if acceleration along the phase encoding direction is employed, one cannot just use images of each slice obtained individually in a single-shot using acceleration along phase encoding direction. Calibration scans are also needed for the phase-encode undersampling and this is typically done using *segmented multi-shot (as opposed to single-shot)* EPI. Segmented EPI sampling of *k*-space is prone to degradation induced by subject motion as well as physiological processes related to respiration and cardiac pulsation [27]; this degradation typically appears in the form of 'ghosting' artifacts, i.e. displacement of signal intensities to regions where they should not be. Respiration can be a source of small rigid body motion of the head but it also affects MR images, especially EPI through perturbations of the B_0 field over the brain caused by alterations of air-filled lung volume during the respiration cycle [45, 46] because air has significantly different magnetic susceptibility than tissue. Cardiac pulsation induces *non*-rigid body motion in the brain, most prominent in ventral parts, particularly in the brainstem.

Thus, a *segmented* EPI acquisition is not necessarily optimal as a calibration scan for unaliasing images obtained with simultaneous acceleration along the slice and phase-encode directions. Instead, we examined the use of standard GRE images, acquiring one *k*-space line after an RF pulse (i.e. FLASH) as a calibration scan, acquired with a lower resolution than the final resolution of the subsequently accelerated data. This approach provided significant improvements and is employed in the 7 Tesla component of the HCP [24, 42] as well as in the 3T Lifespan piloting efforts undertaken within the HCP.

Examples from HCP data

rfMRI came to existence with the observation that functionally related areas that are co-activated in a task (and detected by task fMRI) show correlated spontaneous fluctuations in the absence of any task when the subjects are simply 'resting' in the magnet [7]. This led to the concept that functionally linked areas (though not necessarily all directly connected) exhibit distinct spontaneous oscillations and thus can be extracted from the rfMRI data [47]. Hence it is possible to identify from rfMRI data so called resting-state networks (RSNs) that are classified, for example as 'visual' or 'sensory-motor', or 'language' etc. networks. The identifications are based on the observation that the spatial patterns that are depicted in these RSNs (which resemble activation maps but are actually regions that display temporally-correlated spontaneous fluctuations) have similarities to collection of regions activated by task based fMRI. This is an important observation since it supports the concept that RSNs reflect neuronal processes and not necessarily temporally correlated fluctuations that can be observed in the brain but are not linked to neuronal activity (e.g. [17]).

The HCP fMRI data obtained with slice acceleration and subsequently cleaned by independent component analysis (ICA) based methods [48] provide excellent and convincing demonstration of the correspondence between areas seen in task fMRI and RSNs extracted from ICA analysis of rfMRI time series. They strengthen the argument that regions that are intimately linked functionally do have correlated spontaneous fluctuations even when they are not actively involved in the execution of a task.

Of course, rfMRI data yield many RSNs (in this regard, HCP data are unique in being able to identify a very large number of such RSNs that are much more fine grained than what was previously available [22, 49]). It is not immediately possible to identify an association between all of these RSNs and activation patterns elicited with specific tasks. This is expected. For example, a visuo-motor task, such as moving a joy stick in the direction of a target presented to the subject, will yield a very large number of activated areas in the brain. A single RSN that corresponds to those areas likely is not identified.

4

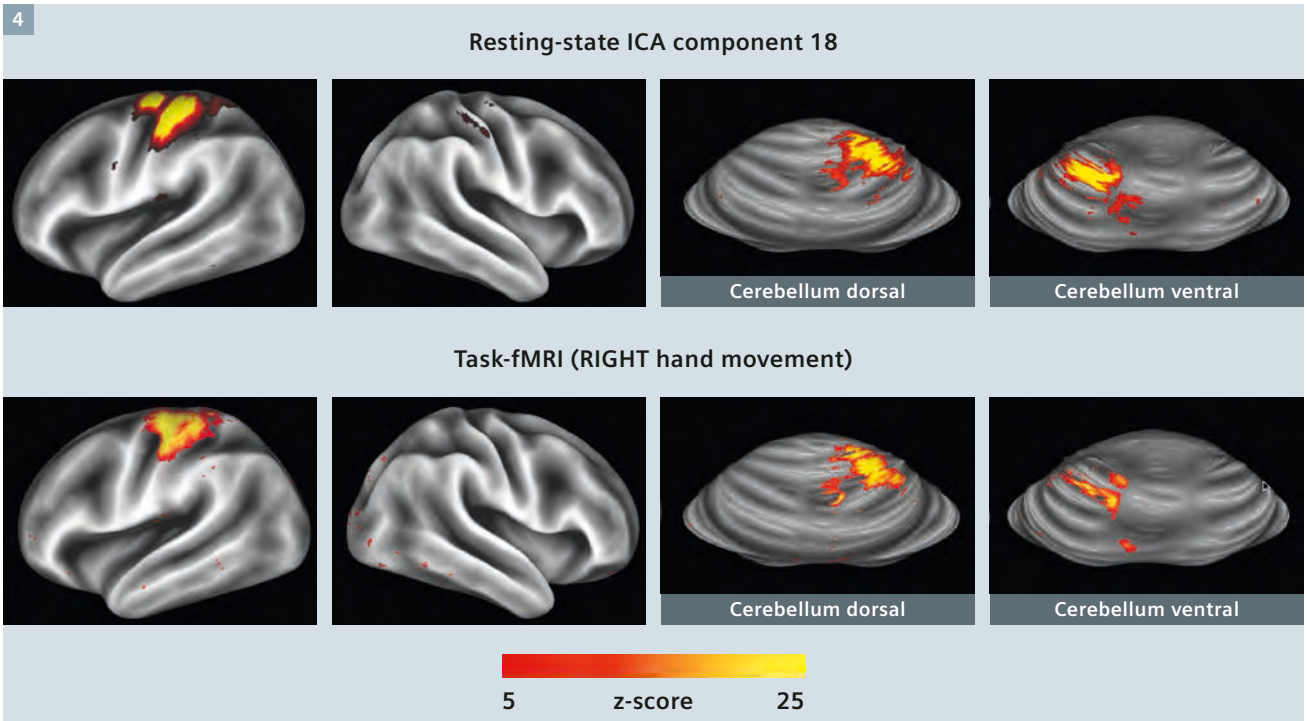

4 Comparison between activation patterns observed with task-fMRI when subjects are performing a simple 'hand task' with the right hand and an ICA component extracted from the resting-state fMRI data from the HCP database. Patterns mapped onto the group-average cerebral surfaces (first two panels) and onto the inflated cerebellar atlas surface that has been mapped to the MNI atlas stereotaxic space [Van Essen, 2009]. Resting-state fMRI component 13 from a 100-dimensional ICA decomposition (with 82 components judged to be signal), applied to the 66 subjects in the HCP Q1 data release having four rfMRI runs. *Adapted from Van Essen et al. 2013 [50].*

5

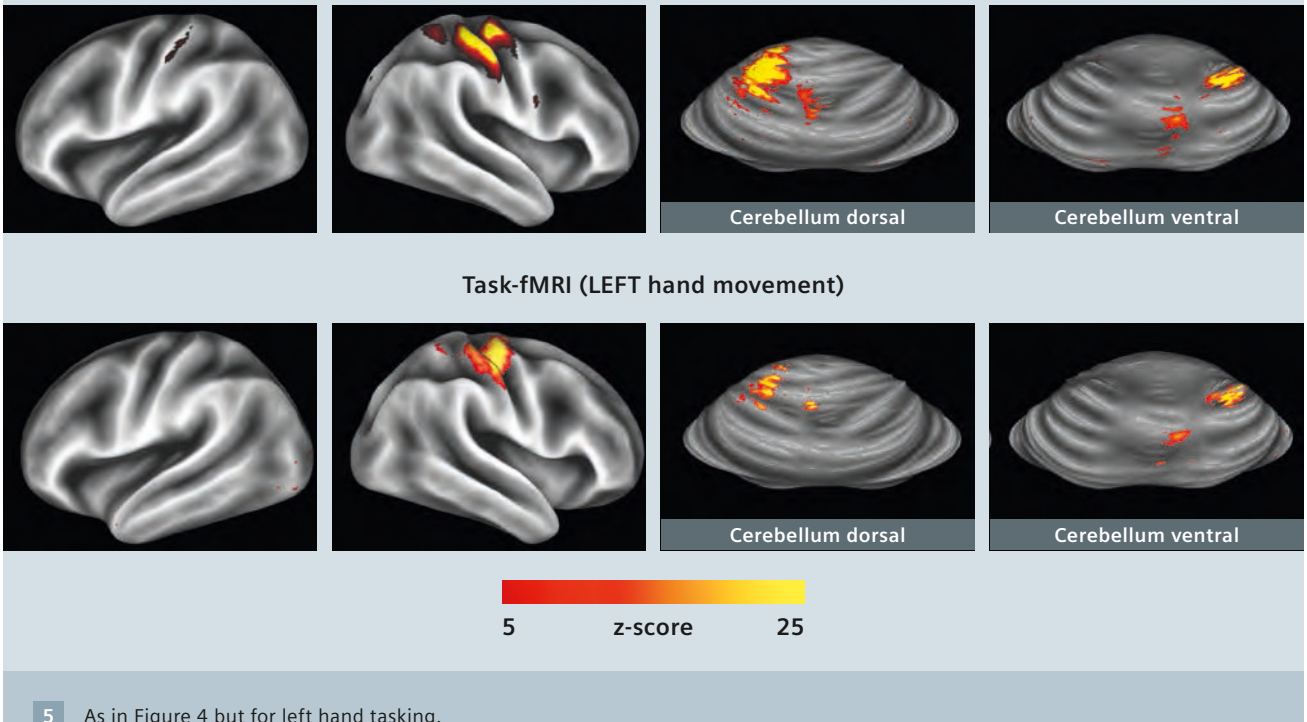

5 As in Figure 4 but for left hand tasking.

Instead, RSNs that represent motor networks, visual networks and others (likely involving parietal areas) together will represent the task induced activation pattern. The collections of RSNs that can explain the activation pattern induced by such a task would yield important information about networks engaged in that task.

However, for simple tasks, it is in fact possible to find correspondence between task based fMRI and an RSN which is an ICA component obtained from the rfMRI. An example from the HCP 3T data is shown in Figure 4, which illustrates this cross-modal comparison with data mapped to a cortical and cerebellar surface map [50]. The bottom row shows the group-average task activation from the right-hand 'hand movement' task, analyzed for a group of 20 unrelated subjects scanned for the HCP database. It includes activation in the expected location in the left motor cortex (left panel), and also at two distinct locations in dorsal and ventral cerebellum, matching published reports [4]. The top row shows a spatially corresponding ICA component from a 100-component group-level ICA-based network decomposition (with 82 'signal' components), carried out on 66 HCP subjects scanned at 3T from the first quarter data release. The correspondence in spatial patterns between the rfMRI ICA component and the task-fMRI activation is striking [50].

Figure 5 illustrates the same for the left hand tasking. Now the cortical and cerebellar hemispheres are expected to be flipped for both the ICA component and task activation pattern; indeed, this is what is observed and again similarities are striking.

Anatomical and functional connectivity data can be probed using a seed based approach, where connectivity derived from rfMRI is represented as a correlation of signal fluctuations of each voxel with the seed voxel, and anatomical connections are represented as a probabilistic connectivity derived from dMRI data of each voxel to the seed voxel. For any given voxel or seed locations, one expects to find similarities between such functional and anatomical connectivity maps. Figure 6 (top row) shows probabilistic streamlines that can be created in the Connectome workbench (Fig. 6A) and probabilistic connectivity represented on the brain surface (Fig. 6B) in a single subject from a seed location placed in the orbitofrontal cortex (location indicated by arrows in Figs. 6A, B). The lower row in Figure 6 compares functional versus structural connectivity on the flattened cortical surface from a group of 9 subjects from the same seed location. Given that the two methods have different limitations and errors, the fact that similar data are obtained in the functional versus the structural connectivity maps is reassuring.

It should be noted, however, that such structural vs. functional connectivity maps (Figs. 6C and D, respectively) need not be identical even if they suffered no errors. In a network,

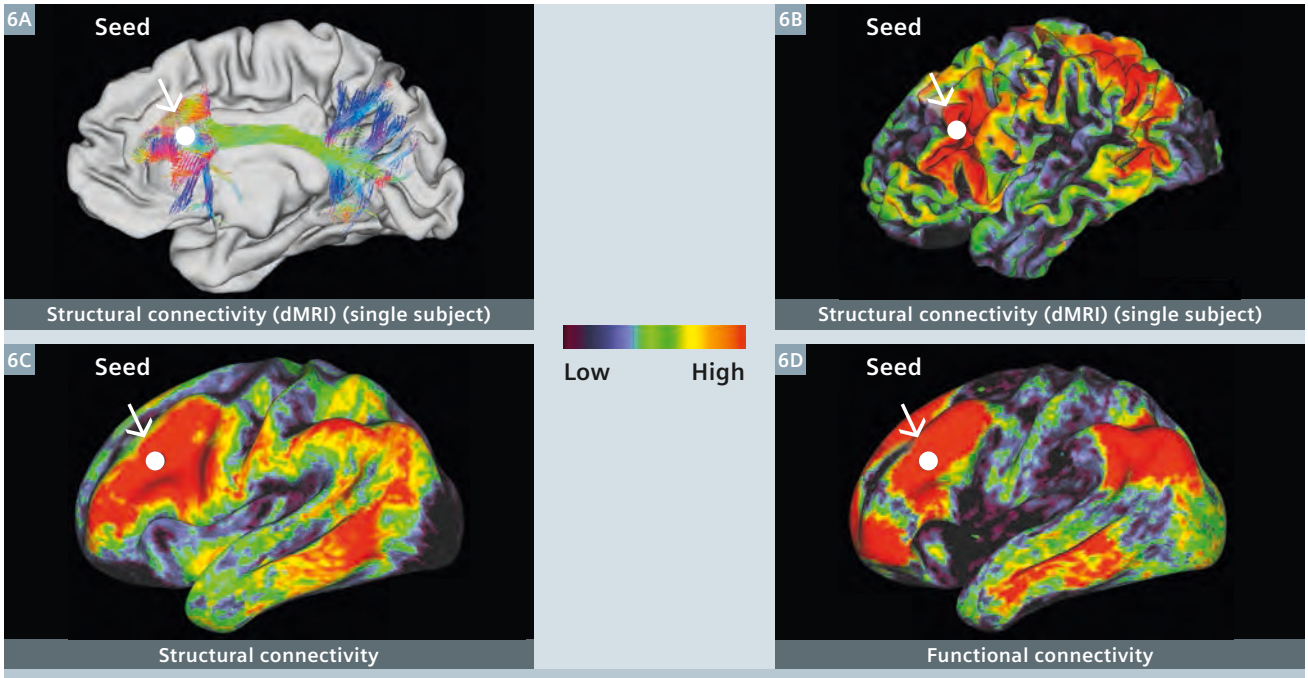

6 Structural connectivity obtained from dMRI versus functional connectivity derived from resting-state fMRI data, in an individual and in group averages. Connectivity trajectory visualization for a single HCP subject (100307). Probabilistic trajectories seeded from a single gray ordinate in left frontal cortex (white dot identified also by an arrow) and intersecting the white/gray matter boundary surface in at least one more location **(6A)**. Probabilistic structural connectivity of the same subject as viewed on the cortical surface **(6B)**. Structural connectivity values in a group average (9 HCP subjects) for the same seed location (white dot), viewed on the inflated cortical surface. The values are displayed using a logarithmic scale **(6C)**. Functional connectivity values for the same seed location, displayed on the inflated surface **(6D)**. The values correspond to the average functional connectivity of a group of 20 HCP subjects. (Note: seed in Panel 6A is not the same as in 6B, C, and D). *Adapted from Van Essen et al., 2013 [50].*

each region does not have to have a direct (anatomical) connection to every other region. For example in a network of 3 nodes, identified as 1,2, and 3, node 1 can be directly connected to node 2 and node 3 but no direct connection exists between nodes 2 and 3. This situation may lead to interesting patterns if we compare the probabilistic 'anatomical connectivity' map derived from the dMRI and the 'functional connectivity' map obtained from rfMRI. In this case, nodes 1, 2, and 3 can still show correlated spontaneous fluctuations. Putting a 'seed' in node 1 to generate such maps should yield identical anatomical and functional connectivity maps; but putting a 'seed' in node 2 or 3 will yield partially overlapping anatomical and functional connectivity maps, reflecting the fact that node 2 and 3 have no direct anatomical connectivity but still display correlated spontaneous fluctuations that have 'functional connectivity', in this case indirectly through another node.

Conclusion

The 3T protocols in the WU-Minn HCP Consortium are now 'frozen' and produce data that are significantly higher quality than what has been possible using conventional methods and instrumentation to date. Nevertheless, intense efforts were still devoted to further methodological developments within the WU-Minn consortium, largely targeting optimization of the 7T HCP data collection and are detailed in [42]. However, the impact of these developments is also anticipated to go well beyond the current HCP and is expected to spread to future efforts at any field strength. Accelerated volume coverage, whether with Multiband/SMS as currently employed in the HCP, or new approaches to be developed, may soon become the default acquisition scheme in fMRI and dMRI studies. The utility of these MR techniques are relevant to potential new initiatives investigating connectomics, for example, in relation to development, life-span, and/or brain diseases. Such initiatives will be able to take full advantage of on-going methodological improvements that would be available at the time of their start.

Acknowledgements

The work reported in this article was supported by the Human Connectome Project (1U54MH091657) from the 16 Institutes and Centers of the National Institutes of Health that support the NIH Blueprint for Neuroscience Research and by Biotechnology Research Center (BTRC) grant P41 EB015894 from NIBIB, and NINDS Institutional Center Core Grant P30 NS076408. The authors would like to thank Siemens Healthcare for collaboration and support during the Human Connectome Project.

References

1 Hagmann P, Cammoun L, Gigandet X, Meuli R, Honey CJ, Wedeen VJ, Sporns O. Mapping the structural core of human cerebral cortex. PLoS Biol 2008;6(7):e159.
2 van den Heuvel MP, Stam CJ, Kahn RS, Hulshoff Pol HE. Efficiency of functional brain networks and intellectual performance. J Neurosci 2009;29(23):7619-7624.
3 Nelson SM, Cohen AL, Power JD, Wig GS, Miezin FM, Wheeler ME, Velanova K, Donaldson DI, Phillips JS, Schlaggar BL, Petersen SE. A parcellation scheme for human left lateral parietal cortex. Neuron 2010;67(1):156-170.
4 Yeo BT, Krienen FM, Sepulcre J, Sabuncu MR, Lashkari D, Hollinshead M, Roffman JL, Smoller JW, Zollei L, Polimeni JR, Fischl B, Liu H, Buckner RL. The organization of the human cerebral cortex estimated by intrinsic functional connectivity. J Neurophysiol 2011;106(3):1125-1165.
5 Mars RB, Jbabdi S, Sallet J, O'Reilly JX, Croxson PL, Olivier E, Noonan MP, Bergmann C, Mitchell AS, Baxter MG, Behrens TE, Johansen-Berg H, Tomassini V, Miller KL, Rushworth MF. Diffusion-weighted imaging tractography-based parcellation of the human parietal cortex and comparison with human and macaque resting-state functional connectivity. J Neurosci 2011;31(11):4087-4100.
6 Power JD, Cohen AL, Nelson SM, Wig GS, Barnes KA, Church JA, Vogel AC, Laumann TO, Miezin FM, Schlaggar BL, Petersen SE. Functional network organization of the human brain. Neuron 2011;72(4):665-678.
7 Biswal B, Yetkin FZ, Haughton VM, Hyde JS. Functional Connectivity in the Motor Cortex of Resting Human Brain Using Echo-Planar Mri. Magnetic Resonance in Medicine 1995;34(4):537-541.
8 Fox MD, Raichle ME. Spontaneous fluctuations in brain activity observed with functional magnetic resonance imaging. Nat Rev Neurosci 2007;8(9):700-711.
9 Vincent JL, Patel GH, Fox MD, Snyder AZ, Baker JT, Van Essen DC, Zempel JM, Snyder LH, Corbetta M, Raichle ME. Intrinsic functional architecture in the anaesthetized monkey brain. Nature 2007;447(7140):83-86.
10 Beckmann CF, DeLuca M, Devlin JT, Smith SM. Investigations into resting-state connectivity using independent component analysis. Philos Trans R Soc Lond B Biol Sci 2005;360(1457):1001-1013.
11 Smith SM, Miller KL, Salimi-Khorshidi G, Webster M, Beckmann CF, Nichols TE, Ramsey JD, Woolrich MW. Network modelling methods for FMRI. Neuroimage 2011;54(2):875-891.
12 Mori S, Zhang J. Principles of diffusion tensor imaging and its applications to basic neuroscience research. Neuron 2006;51(5):527-539.
13 Jbabdi S, Johansen-Berg H. Tractography: where do we go from here? Brain connectivity 2011;1(3):169-183.
14 Iturria-Medina Y, Sotero RC, Canales-Rodriguez EJ, Aleman-Gomez Y, Melie-Garcia L. Studying the human brain anatomical network via diffusion-weighted MRI and Graph Theory. Neuroimage 2008;40(3):1064-1076.
15 Uludag K, Muller-Bierl B, Ugurbil K. An integrative model for neuronal activity-induced signal changes for gradient and spin echo functional imaging. Neuroimage 2009;48(1):150-165.
16 Iadecola C. Neurovascular regulation in the normal brain and in Alzheimer's disease. Nat Rev Neurosci 2004;5(5):347-360.
17 Mitra PP, Ogawa S, Hu X, Ugurbil K. The nature of spatiotemporal changes in cerebral hemodynamics as manifested in functional magnetic resonance imaging. Magn Reson Med 1997;37(4):511-518.
18 Panagiotaki E, Schneider T, Siow B, Hall MG, Lythgoe MF, Alexander DC. Compartment models of the diffusion MR signal in brain white matter: a taxonomy and comparison. NeuroImage 2012;59(3):2241-2254.
19 Van Essen DC, Jbabdi S, Sotiropoulos SN, Chen C, Dikranian K, Coalson T, John Harwell J, Behrens TEJ, Glasser MF. Mapping Connections in Humans and Nonhuman Primates: Aspirations and Challenges for Diffusion Imaging. Diffusion MRI (2nd Edition); 2013.
20 Van Essen DC, Smith SM, Barch DM, Behrens TE, Yacoub E, Ugurbil K, for the WU-Minn HCP Consortium. The WU-Minn Human Connectome Project: An overview. Neuroimage 2013;80:62-79.
21 Sotiropoulos SN, Jbabdi S, Xu J, Andersson JL, Moeller S, Auerbach EJ, Glasser MF, Hernandez M, Sapiro G, Jenkinson M, Feinberg DA, Yacoub E, Lenglet C, Van Essen DC, Ugurbil K, Behrens TE, for the

WU-Minn HCP Consortium. Advances in diffusion MRI acquisition and processing in the Human Connectome Project. Neuroimage 2013;80:125-143.
22 Smith SM, Beckmann CF, Andersson J, Auerbach EJ, Bijsterbosch J, Douaud G, Duff E, Feinberg DA, Griffanti L, Harms MP, Kelly M, Laumann T, Miller KL, Moeller S, Petersen S, Power J, Salimi-Khorshidi G, Snyder AZ, Vu AT, Woolrich MW, Xu J, Yacoub E, Ugurbil K, Van Essen DC, Glasser MF, for the WU-Minn HCP Consortium. Resting-state fMRI in the Human Connectome Project. Neuroimage 2013;80:144-168.
23 Glasser MF, Sotiropoulos SN, Wilson JA, Coalson TS, Fischl B, Andersson JL, Xu J, Jbabdi S, Webster M, Polimeni JR, Van Essen DC, Jenkinson M, Consortium WU-MH. The minimal preprocessing pipelines for the Human Connectome Project. Neuroimage 2013;80:105-124.
24 Ugurbil K, Xu J, Auerbach EJ, Moeller S, Vu AT, Duarte-Carvajalino JM, Lenglet C, Wu X, Schmitter S, Van de Moortele PF, Strupp J, Sapiro G, De Martino F, Wang D, Harel N, Garwood M, Chen L, Feinberg DA, Smith SM, Miller KL, Sotiropoulos SN, Jbabdi S, Andersson JL, Behrens TE, Glasser MF, Van Essen DC, Yacoub E, for the WU-Minn HCP Consortium. Pushing spatial and temporal resolution for functional and diffusion MRI in the Human Connectome Project. Neuroimage 2013;80:80-104.
25 Barch DM, Burgess GC, Harms MP, Petersen SE, Schlaggar BL, Corbetta M, Glasser MF, Curtiss S, Dixit S, Feldt C, Nolan D, Bryant E, Hartley T, Footer O, Bjork JM, Poldrack R, Smith S, Johansen-Berg H, Snyder AZ, Van Essen DC, Consortium WU-MH. Function in the human connectome: Task-fMRI and individual differences in behavior. Neuroimage 2013;80:169-189.
26 Moeller S, Yacoub E, Olman CA, Auerbach E, Strupp J, Harel N, Ugurbil K. Multiband multislice GE-EPI at 7 tesla, with 16-fold acceleration using partial parallel imaging with application to high spatial and temporal whole-brain fMRI. Magn Reson Med 2010;63(5):1144-1153.
27 Moeller S, Auerbach E, van de Moortele P-F, Adriany G, Ugurbil K. fMRI with 16 fold reduction using multibanded multislice sampling. Proc Int Soc Mag Reson Med 2008;16:2366.
28 Larkman DJ, Hajnal JV, Herlihy AH, Coutts GA, Young IR, Ehnholm G. Use of multicoil arrays for separation of signal from multiple slices simultaneously excited. J Magn Reson Imaging 2001;13(2):313-317.
29 Breuer FA, Blaimer M, Heidemann RM, Mueller MF, Griswold MA, Jakob PM. Controlled aliasing in parallel imaging results in higher acceleration (CAIPIRINHA) for multi-slice imaging. Magn Reson Med 2005;53(3):684-691.
30 Breuer FA, Blaimer M, Mueller MF, Seiberlich N, Heidemann RM, Griswold MA, Jakob PM. Controlled aliasing in volumetric parallel imaging (2D CAIPIRINHA). Magn Reson Med 2006;55(3):549-556.
31 Nunes RG, Hajnal JV, Golay X, Larkman DJ. Simultaneous slice excitation and reconstruction for single shot EPI. Proc Int Soc Mag Reson Med 2006;14:293.
32 Setsompop K, Gagoski BA, Polimeni J, Witzel T, Wedeen VJ, Wald LL. Blipped CAIPIRINHA for simultaneous multi-slice EPI with reduced g-factor penalty. Proc Int Soc Mag Reson Med 2010;18:551.
33 Setsompop K, Gagoski BA, Polimeni JR, Witzel T, Wedeen VJ, Wald LL. Blipped-controlled aliasing in parallel imaging for simultaneous multislice echo planar imaging with reduced g-factor penalty. Magn Reson Med 2012;67(5):1210-1224.
34 Feinberg DA, Reese TG, Wedeen VJ. Simultaneous echo refocusing in EPI. Magn Reson Med 2002;48(1):1-5.
35 Feinberg DA, Moeller S, Smith SM, Auerbach E, Ramanna S, Gunther M, Glasser MF, Miller KL, Ugurbil K, Yacoub E. Multiplexed echo planar imaging for sub-second whole brain FMRI and fast diffusion imaging. PLoS ONE 2010;5(12):e15710.
36 Xu J, Moeller S, Auerbach EJ, Strupp J, Smith SM, Feinberg DA, Yacoub E, Ugurbil K. Evaluation of slice accelerations using multiband echo planar imaging at 3 T. Neuroimage 2013;83:991-1001.
37 Pruessmann KP, Weiger M, Scheidegger MB, Boesiger P. SENSE: sensitivity encoding for fast MRI. Magn Reson Med 1999;42(5):952-962.
38 Moeller S, Xu J, Auerbach EJ, Yacoub E, Ugurbil K. Signal Leakage(L-factor) as a measure for parallel imaging performance among simultaneously multi-Slice (SMS) excited and acquired signals. Proc Int Soc Mag Reson Med 2012;20:519.
39 Auerbach EJ, Xu J, Yacoub E, Moeller S, Ugurbil K. Multiband accelerated spin-echo echo planar imaging with reduced peak RF power using time-shifted RF pulses. Magn Reson Med 2013;69(5):1261-1267.
40 Wu X, Schmitter S, Auerbach EJ, Ugurbil K, Van de Moortele PF. A generalized slab-wise framework for parallel transmit multiband RF pulse design. Magn Reson Med 2015.
41 Wu X, Schmitter S, Auerbach EJ, Moeller S, Ugurbil K, Van de Moortele PF. Simultaneous multislice multiband parallel radio-frequency excitation with independent slice-specific transmit B1 homogenization. Magn Reson Med 2013;70(3):630-638.
42 Vu AT, Auerbach E, Lenglet C, Moeller S, Sotiropoulos SN, Jbabdi S, Andersson J, Yacoub E, Ugurbil K. High resolution whole brain diffusion imaging at 7T for the Human Connectome Project. Neuroimage 2015;122:318-331.
43 Andersson JL, Sotiropoulos SN. Non-parametric representation and prediction of single- and multi-shell diffusion-weighted MRI data using Gaussian processes. Neuroimage 2015;122:166-176.
44 Andersson JL, Skare S, Ashburner J. How to correct susceptibility distortions in spin-echo echo-planar images: application to diffusion tensor imaging. Neuroimage 2003;20(2):870-888.
45 Pfeuffer J, Van De Moortele PF, Ugurbil K, Hu X, Glover GH. Correction of physiologically induced global off-resonance effects in dynamic echo-planar and spiral functional imaging. Magn Reson Med 2002;47(2):344-353.
46 Van De Moortele PF, Pfeuffer J, Glover GH, Ugurbil K, Hu X. Respiration-induced B0 fluctuations and their spatial distribution in the human brain at 7 Tesla. Magn Reson Med 2002;47(5):888-895.
47 Smith SM, Fox PT, Miller KL, Glahn DC, Fox PM, Mackay CE, Filippini N, Watkins KE, Toro R, Laird AR, Beckmann CF. Correspondence of the brain's functional architecture during activation and rest. Proc Natl Acad Sci U S A 2009; 106(31):13040-13045.
48 Griffanti L, Salimi-Khorshidi G, Beckmann CF, Auerbach EJ, Douaud G, Sexton CE, Zsoldos E, Ebmeier KP, Filippini N, Mackay CE, Moeller S, Xu J, Yacoub E, Baselli G, Ugurbil K, Miller KL, Smith SM. ICA-based artefact removal and accelerated fMRI acquisition for improved resting state network imaging. Neuroimage 2014;95:232-247.
49 Smith SM, Vidaurre D, Beckmann CF, Glasser MF, Jenkinson M, Miller KL, Nichols TE, Robinson EC, Salimi-Khorshidi G, Woolrich MW, Barch DM, Ugurbil K, Van Essen DC. Functional connectomics from resting-state fMRI. Trends Cogn Sci 2013;17(12):666-682.

Contact

Kâmil Uğurbil, Ph.D.
Director Center for Magnetic Resonance Research
Department of Radiology 1-211C CMRR
University of Minnesota
2021 Sixth Street SE
Minneapolis, MN 55455, USA
Phone: +1 612-626-9591
kamil@cmrr.umn.edu